Aalborg Universitet

AALBORG UNIVERSITY

Path-Loss Prediction for an Industrial Indoor Environment Based on Room Electromagnetics

Ai, Yun ; Andersen, Jørgen Bach; Cheffena, Michael

Path-Loss Prediction for An Industrial Indoor Environment Based on Room Electromagnetics

Yun Ai, *Student Member, IEEE,* Jørgen Bach Andersen, *Life Fellow, IEEE,* and Michael Cheffena

Abstract—A simple approach of path-loss and root mean square delay spread prediction for indoor propagation environment is developed based on the room electromagnetics theory. The indoor room environment is interpreted as a lossy cavity, which is characterized by the diffuse scattering components caused by the walls and surrounding obstacles, and a possible line-of-sight component. Simplicity, speed of the algorithm and good accuracy are among the advantages of this approach. To apply the method, it only requires the knowledge of the dimensions of the room and the reverberation time, which can be easily obtained from one measurement of the power-delay-profile in the investigated environment. For experimental validation, path-loss measurements at two different transmission frequencies, and wideband measurements from 0.8 to 2.7 GHz were conducted in two rooms of an industrial environment. The theoretical results from the path-loss and root mean square delay spread prediction algorithm show good match with the measurement results.

Index Terms—Channel measurement, UWB propagation, power-delay-profile, path-loss, diffuse scattering, room acoustics, room electromagnetics.

I. INTRODUCTION

The successful design and deployment of wireless systems requires a good knowledge of the propagation characteristics of the channel. To this end, the channel models for various scenarios have been the topic of research for many years [1]–[3]. In order to analyze the wireless channel, path-loss is considered to be one of the most important characteristics. Path-loss analysis provide knowledge on the power density reduction of the electromagnetic waves as they propagate through space in a specific environment, important for analyzing the channel capacity and radio coverage of a wireless network [4]–[6].

This paper focuses on the prediction of radio wave propagation in indoor environments, with application to wireless communication systems in the centimeter-wave frequency range. There exist different approaches to predict the path-loss. A number of empirical models for path-loss were derived based on field measurements in various environments [6]–[8]. The measurement campaigns required for deriving these models usually mean a lot of cost in time and manpower. Moreover, the nature of empirical models implies that they are only applicable and accurate for environments sharing the same

propagation characteristics with those where the measurements were performed, which limits the usage of empirical channel models. Some simple statistical models for path-loss modeling have been proposed for standardization in [9]–[11], which assume a finite number of rays (plane waves). The path-loss prediction model in this paper only assumes uniform angular distribution and that the line-of-sight (LOS) part exists which is followed by diffuse components. These assumptions were also verified by the numerical models proposed in [12]–[14].

Ray tracing (RT) is an alternative channel modeling technique, which evaluates all propagation paths as they interact with the surrounding environment based on the geometrical optics and uniform theory of diffraction [15]–[17]. Taking into consideration the most widely used centimeter-wave frequency range of wireless communication systems and the roughness of reflectors and scatterers in common rooms (especially in indoor environments such as industrial rooms), we consider diffuse scattering to be more important than coherent scattering from smooth surfaces (such as smooth walls), if not crucial. However, the accuracy of the RT simulations strongly depends on the implemented mathematical models as well as on the data used to describe the environment. In addition, simulation of diffuse scattering components using RT algorithms often
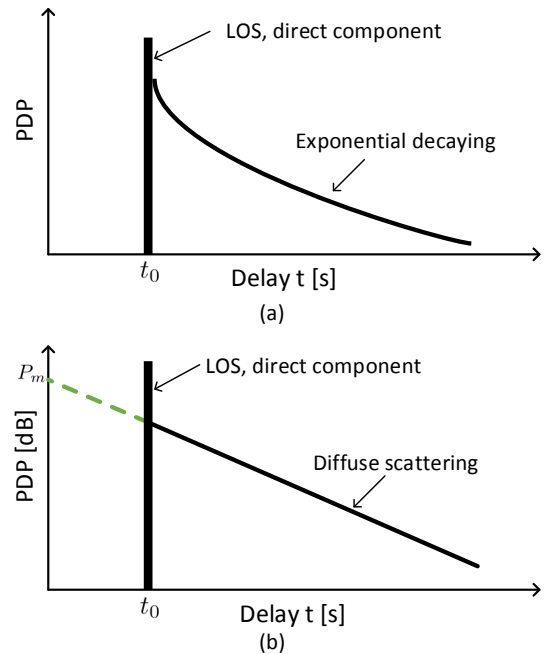

Fig. 1: (a). Power-delay-profile (PDP) in linear unit versus propagation delay; (b). PDP in decibel unit versus propagation delay.

leads to large, sometimes prohibitive, computational cost and simulation time [18].

In a recent work [19], the room electromagnetics theory was proposed based on purely diffuse scattering analogous to the "room acoustics" theory. The theory was motivated by the similarity of the wavelengths for both audio waves and microwaves, whereas the size of the room and the roughness of the walls and scatterers are expected to produce similar reverberation effects throughout the room. The acoustic community has applied the "room acoustics" and the underlying Sabine's equation to predict the sound field in a room since 1920s. The key idea of the theory is to consider the indoor room environment as a lossy cavity, which is characterized by the LOS component and diffuse scattered components resulting from the walls and other internal obstacles. The diffuse scattering leads to a tail with exponential decay, which translates into a linear relationship when expressed in decibel unit (see Fig. 1). The extension from the acoustic wave to the electromagnetic wave is feasible since the fundamental difference between them is only the polarization. The acoustic waves are longitudinal while the electromagnetic waves are transverse and hence exhibit polarization effects.

The room electromagnetics theory has been previously applied for the electromagnetic field analysis of scenarios such as offices [12], [20], [21], seminar room [22], and aircraft cabin [2]. Different from the aforementioned environments, the industrial facility investigated in this paper presents a highly dense scattering environment with several strongly reflective objects. The industrial room is also featured as a radio-harsh environment with high noise level, intensive interference, etc. This paper will investigate whether the room electromagnetics theory is valid in such an environment and apply the simple but effective theory for our purpose of path-loss prediction.

The remainder of the paper is organized as follows: Section II briefly introduces the room electromagnetics method and its application for the purpose of path-loss and rms delay profile estimation. Section III describes the measured industrial environments and the measurement setup. Section IV discusses the wideband and path-loss measurement results and the theoretical results obtained from the path-loss prediction method. Finally, summary and conclusion are drawn in Section V.

II. ROOM ELECTROMAGNETICS BASED PREDICTION APPROACH

In this section, we derive the expressions of the path-loss and root mean square (rms) delay spread based on the room electromagnetics theory. The flow chart illustrating the methodology for the path-loss prediction algorithm is given.

A. Path-Loss Prediction

Electromagnetic waves may be reflected by rough walls and obstacles in two ways, i.e., (i) a coherent component, which for planar structures can be computed with the image theory and the Fresnel reflection coefficients, and (ii) an incoherent scatter from all scatterers in all directions. The reflection coefficient has an inverse proportional relationship with the roughness of the wall. It is assumed that the roughness (or randomness) is

so large that the diffuse component dominates. This leads to an exponential decay of power with a decay constant τ, which is termed as reverberation time and is expressed from (A-8) as

$$\tau = \frac{4V}{cA'} = \frac{4V}{cA\eta},$$ (1)

where c is the speed of light, A and V are the surface area and the volume of the investigated room, respectively, the absorption ratio η is defined as the ratio between the effective absorption area A' and the surface area A. The reverberation time τ is also linked to the slope of the power-delay-profile (PDP) in dB according to (A-9) and can be readily obtained from one measurement of the PDP. It should be noted that it is clear that the reverberation time will in principle be frequency dependent [23], but as will be shown later in Section III, in the present case the frequency range from 800 MHz to 2.7 GHz is too limited to reveal a possible frequency dependence in the present environments. This frequency independence phenomenon over a large frequency band has also been confirmed by recent reverberation time measurements in university laboratories of the Universidad Politecnica de Cartagena (UPCT) in Spain [23]. It was observed that there is insignificant relative deviation of reverberation time over frequency bands up to 900 MHz (or more) in the UPCT measurements (see Fig. 3 of [23]), which indicates that the reverberation time in the measured environments can be considered as constant over bands up to 900 MHz (or more) for frequencies from 2 to 10 GHz. This is probably due to the fact that the properties of materials present in the environments do not vary significantly over a wide frequency range [24]. In this case, we can just divide the relatively wide frequency band from 2 to 10 GHz into several subbands, wherein the reverberation time can be considered as constant within each subband and then analyze each of the subbands using the proposed room electromagnetics approach.

Then, the power resulting from the diffuse components can be expressed according to (A-14) as follows:

$$P_{dif} = \frac{\lambda^2 w}{8\pi^2 A\eta} \cdot e^{-\frac{d}{c\tau}},$$ (2)

where λ is the wavelength, w represents the width of a rectangular pulse of unit amplitude, and d is the distance between the transmitter (Tx) antenna and the receiver (Rx) antenna.

Normalizing the received power in (2) with the input power $P_{in} = 1^2 \cdot w = w$ and utilizing the relationship in (1), we obtain the path-loss in dB under the non-line-of-sight (NLOS) scenario as a function of the Tx-Rx distance d and frequency f as follows:

$$PL(d, f) = 10 \cdot \left[\log_{10}\left(\frac{32\pi^2 f^2 V}{c\tau}\right) - \log_{10}\left(c^2 \cdot \exp\left(\frac{-d}{c\tau}\right)\right) \right].$$ (3)

For the LOS scenario, there exists a direct link between the Tx and Rx, thus a strong line-of-sight field appears besides the diffuse field. The received power corresponding to the LOS component from the Tx antenna is [25]

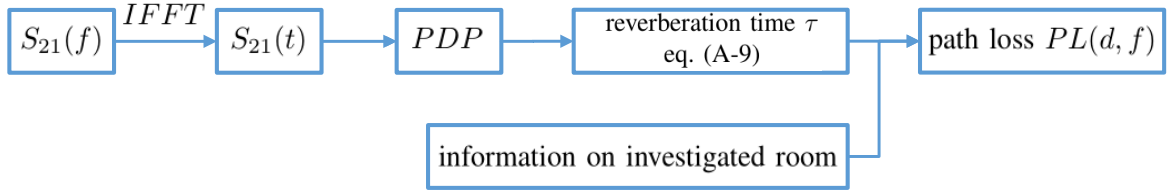$$P_{dir} = \frac{P_{in}D_t D_r c^2}{(4\pi f d)^2},$$ (4)

Fig. 2: Flow chart illustrating the methodology for the path-loss prediction algorithm.
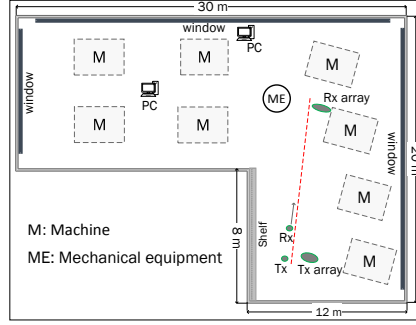

Fig. 3: Measured mechanical room.

Fig. 4: Schematic of the mechanical room.

Fig. 5: Measured electronics room.

where D_t and D_r are the directivities of the Tx and Rx antennas, respectively.

Normalizing the total received power $(P_{dir} + P_{dif})$ with the input power and taking the logarithm, we obtain the following expression for the path-loss in dB in terms of the Tx-Rx distance d and frequency f under the LOS scenario:

$$PL(d,f) = 10 \cdot \log_{10}\left[\left(\frac{c^3\tau}{32\pi^2 f^2 V} \cdot \exp\left(\frac{-d}{c\tau}\right) + \frac{D_t D_r c^2}{(4\pi f d)^2}\right)^{-1}\right]$$
(5)

We can see from (3) and (5) that to determine the average path-loss at a Tx-Rx distance d and frequency f, we just need to have the knowledge of the volume V and the reverberation time τ. The volume V can be easily known from the dimensions of the room and the absorptive or reflecting objects. The reverberation time τ is obtained from the slope of the measured impulse response according to (A-9). Moreover, if one does not have the capability to conduct wideband measurement to extract the PDP, it is still possible to do the path-loss estimation using the algorithm. In that case, the absorption ratio can be roughly estimated by looking into the absorptive objects and absorbing walls present in the investigated room and their electromagnetic characteristics [26]. Using the estimated absorption ratio, an approximate reverberation time can be obtained according to (1). However, it is often difficult to give an accurate estimate of the absorption ratio in general cases, especially when the room is a highly occupied and highly scattering environment with various objects like industrial scenarios. The advantage of the room electromagnetics approach lies in its simplicity and the fact that the required parameters for the algorithm are extremely easy to obtain. A flow chart which illustrates the methodology for the path-loss estimation is shown in Fig. 2, where the S_{21} parameter will be introduced in the next section.

Differentiating the path-loss in (3) with respect to the Tx-Rx distance d, we obtain the increase rate of path-loss due to diffuse scattering along with Tx-Rx distance as

$$\frac{\partial PL(d,f)}{\partial d} = \frac{\partial \cdot \left[-10 \cdot \log_{10}(\exp(-\frac{d}{c \cdot \tau}))\right]}{\partial d} = \frac{10}{\ln(10) \cdot \tau c}.$$
(6)

It can be seen from (6) that the slope is only determined by the reverberation time given in (1).

B. Root Mean Square Delay Spread Prediction

We first express the PDP $A_c(t)$ in time domain, which, from (4) and (A-14), can be written as

$$A_c(t) = \frac{P_{in}D_t D_r \lambda^2}{(4\pi d)^2} \cdot \delta\left(t - \frac{d}{c}\right) + \frac{P_{in}\lambda^2 \cdot \exp\left(-\frac{t}{\tau}\right)}{8\pi^2 A\eta\tau} \cdot \mathbb{1}\left(t \geq \frac{d}{c}\right),$$
(7)

where $\delta(\cdot)$ is the delta function and $\mathbb{1}(\cdot)$ is the indicator function.

Then, the mean delay $u_t(d)$ at the Tx-Rx distance d can be expressed in terms of the K-factor from Appendix B as

$$u_t(d) = \frac{d}{c} + \frac{P_{dif}}{P_{dir} + P_{dif}} \cdot \tau = \frac{d}{c} + \frac{\tau}{K+1},$$
(8)

where P_{dif} is the diffuse power in (2), P_{dir} is the power from the LOS component given in (4), τ is the reverberation time, and the Ricean K-factor K is estimated on the basis of the room electromagnetics theory as follows:

$$K = \frac{D_t D_r A \cdot \eta}{2d^2} \cdot \exp\left(\frac{d}{c\tau}\right).$$
(9)

Finally, the rms delay spread $\sigma_t(d)$ at the Tx-Rx distance d can also be written in terms of the Ricean K-factor and reverberation time τ from Appendix B as

$$\sigma_t(d) = \frac{\tau}{\sqrt{K+1}} = \frac{\tau}{\sqrt{\frac{D_t D_r A \cdot \eta}{2d^2} \cdot \exp\left(\frac{d}{c\tau}\right) + 1}}.$$
(10)

From (10), it can be concluded that the rms delay spread will be equal to the reverberation time while the fading channel is totally Rayleigh and the delay spread will be smaller than the reverberation time when the Ricean K-factor is not 0.

III. MEASUREMENT CAMPAIGN

It is clear from Section II that the room electromagnetics based prediction approach depends on the model parameters extracted from a wideband measurement. In order to validate the derived model, both wideband and narrowband measurements are conducted in an industrial facility in Gjøvik, Norway. The narrowband path-loss measurements are done to validate the prediction model.

In this section, we first provide information on the measured environments. Then, the measurement setup for the wideband and narrowband measurements are described.

A. Measurement Environment Description

Observations from a large number of modern factories show that there are certain physical characteristics common to most industrial environments. Generally, industrial buildings are taller than ordinary office or residential buildings and are sectioned into several working areas. Between the working areas, there usually exist straight aisles for passing people or materials. Modern factories usually have perimeter walls made of concrete or steel. The ceilings are often made of metal and supported with intricate metal supporting trusses. Overall, the industrial environments present a much densely scattered scenario than office or residual environments.

The measurements were performed in the mechanical room and the electronics room of a manufacturing factory in Gjøvik, Norway. The one-storied mechanical room occupies an area of around 20 x 30 m^2 with a height of around 6 meters, leading to an empty room volume of approximately 2736 m^3. It has concrete floors and concrete ceilings supported by steel truss work. The room houses several big metallic machines and consists of several metal pipes off the roof. Additionally, a big shelf holding manufacturing components is placed near the position of the Tx during the measurement campaign. Overall, the measured industrial inventory presents a much more densely scattered environment than ordinary office environments. Figure 3 gives an impression on the measured mechanical room and the schematic in Fig. 4 illustrates the placement of the measurement antennas. The electronics room is slightly smaller with an area of about 18 × 27 m^2 and a height of around 5 meters giving an empty room volume of approximately 2430 m^3. It houses two rows of medium-size machinery with a lot of metallic valves present (see Fig. 5).

B. Measurement Setup

1) Wideband Measurement: The Rohde & Schwarz ZNB vector network analyzer (VNA) measures the S_{21} parameter, which was used to extract the complex channel transfer function H(f) within the measured frequency range (i.e., 800 MHz to 2.7 GHz in our measurement campaign). The wireless channel was probed at 600 points within the measured
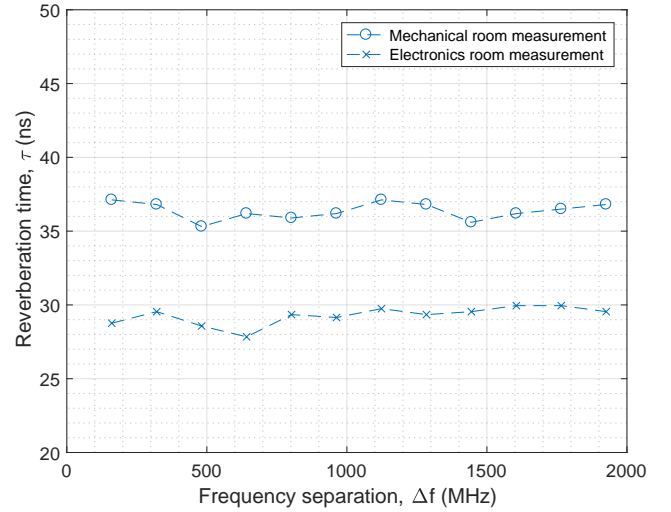

Fig. 8: Reverberation time as a function of frequency separation in the two measured industrial environments.

frequency band, which indicates a separation of 3.21 MHz between two adjacent frequency points. This measurement configuration implies a maximum resolvable delay of around 320 ns and a delay resolution of about 0.526 ns. The swept-frequency signal generated by the VNA was transmitted by an omnidirectional, vertically polarized broadband antenna and received by an antenna of the same type. Both the Tx and Rx antennas were placed 1.8 meters above the ground, which is the height of the machines in the measured industrial room. The wideband measurements were conducted at three different Tx-Rx distances, i.e., $d = 7, 12, 16$ m.

After obtaining the frequency-domain channel transfer function $H(f)$, the channel transfer function is filtered by a Hanning window h_w to reduce aliasing. Next, it is converted to the delay domain using Inverse Discrete Fourier Transform (IDFT) and leads to an instantaneous PDP $A_c(t)$, which we will refer to as local PDP hereinafter. This process is mathematically expressed as

$$A_c(t) = \left| \frac{1}{N_f} \sum_{n=1}^{N_f} [H(f) \times h_w] \cdot \exp(j2\pi f_n \cdot t) \right|^2, \quad (11)$$

where N_f is the number of frequency bins.

2) Path-Loss Measurement: The path-loss measurement system consists of a Rohde & Schwarz SMBV 100A signal generator, a Rohde & Schwarz FSV spectrum analyzer, and the two same omni-directional antennas used in the wideband measurement setup discussed above. The frequencies of the transmitted signals are 1600 MHz and 2450 MHz. The TX was injected with constant input power of 10 dBm and placed at a fixed position while the RX was moved following a straight trajectory, along which samples were taken at Tx-Rx distance from 2 with a step size of 0.5 meter. Altogether 20 measurements at each Rx position were conducted to allow for the removal of the shadowing effect.

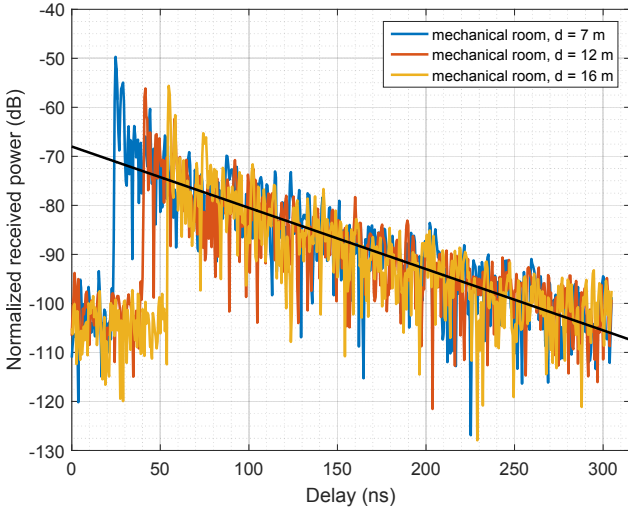The obtained path-loss measurements are also fitted accord-

Fig. 6: Measured PDP for three different Rx positions in the mechanical room.

Fig. 7: Measured PDP for LOS and NLOS scenarios in the electronics room.

ing to the following one-slope model:

$$PL(d) = PL_0 + 10\,n \cdot \log_{10}\Big(\frac{d}{d_0}\Big) + \chi_\sigma, \qquad (12)$$

where n is the path-loss exponent, which reflects the rate at which the received power decreases with distance. The constant PL_0 is an intercept related to the attenuation at the reference distance $d_0 = 2\,\mathrm{m}$. The parameter χ_σ is generally modeled as a zero-mean Gaussian random variable with standard deviation σ when expressed in decibel scale.

IV. Theoretical Analysis of Measurements

In this section, we first extract the model parameters of the investigated environments used for the room electromagnetics prediction method. Followingly, the path-loss and rms delay spread are predicted using the extracted parameters and also compared with the measurements.

A. Model Parameter Extraction

We first extract the parameters required for the room electromagnetics based model from the wideband measurement results. PDP represents the received power associated with a given multipath delay [27]. The measured PDPs at three different Rx positions (all in LOS scenarios) in the mechanical room are shown in Fig. 6. The PDPs were normalized to the input power and hence included the path-loss. The three PDPs have different arrival times owing to the different Tx-Rx distances. Considerable variability is present in the curves due to the lack of spatial averaging in the PDPs. Despite the different arrival time and variability, we can clearly see that the three tails of the PDPs are the same, which have both the same slope and the amplitude. This is in accordance with the general diffuse theory [12], which implies that the tail of the diffuse component is approximately the same regardless of the measured position. The solid straight line in Fig. 6 is obtained by applying the least square fit to all three curves between 100 ns and 260 ns to exclude the effects of the LOS
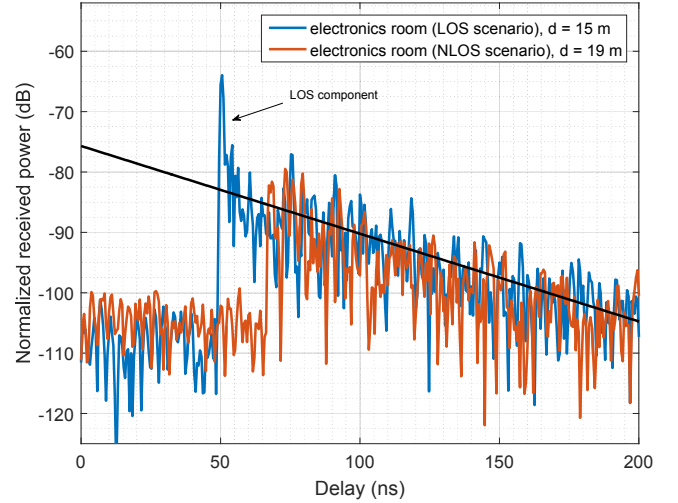
component and the noise floor. The decay rate of the straight line is about 0.12 dB/ns, which corresponds to a reverberation time of around $\tau = 36$ ns.

Figure 7 shows the PDPs at two Tx-Rx distances $d = 16\,\mathrm{m}$ (LOS scenario) and $d = 19\,\mathrm{m}$ (NLOS scenario) in the measured electronics room. The LOS component is clearly present for the PDP corresponding to the $d = 16\,\mathrm{m}$ measurement while the LOS component is absent for the PDP measured at $d = 19\,\mathrm{m}$. It is also interesting to notice the slightly different noise floors in the two different propagation scenarios. However, despite the differences in the overall shapes of the PDPs and the noise floors, we can clearly see that the tails of the two PDPs are almost the same. This is in agreement with the diffuse theory since the slope of the tail is only determined by the diffuse scattering regardless the presence of direct link. The slope of the decaying tail in Fig. 7 is about 0.15 dB/ns, which translates to a reverberation time of around 30 ns.

Figure 8 shows the reverberation time as a function of frequency separation in the investigated industrial scenarios. Different frequency bandwidth from 160.5 MHz up to 1.9 GHz with a step size of 160.5 MHz (3.21 MHz $\times$ 50) in the frequency range 800 MHz to 2.7 GHz are investigated. The maximum relative standard deviations are around 1.6% and 2.1% for the mechanical room and electronics room, respectively. These insignificant deviations imply that the reverberation times can be considered as constant within the investigated frequency band for the two investigated industrial rooms, which is in accordance with reverberation time measurements in other environments [23]. The measured reverberation times in the industrial scenarios are significantly larger than those from the office environment [28]. This is due to the larger area of the industrial facility as well as the presence of dense scatterers in the industrial environment, which makes the tail slope of the PDP much smaller and thus leads to a larger value of reverberation time according to (A-9). In the next section, we will use the reverberation times estimated from the PDPs for our analysis of the path-loss.
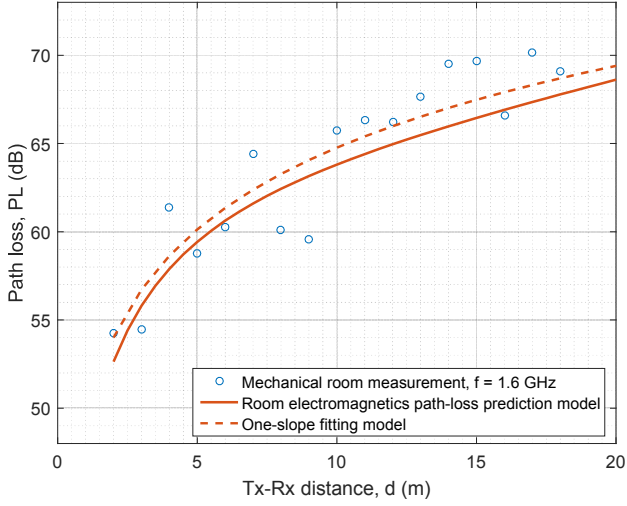
Fig. 9: Path-loss versus the Tx-Rx distance in the measured mechanical room at the frequency $f = 1.60\,\mathrm{GHz}$.
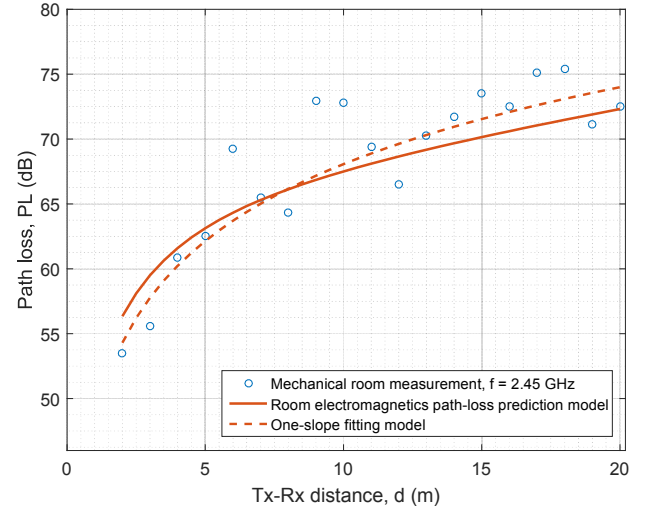

Fig. 10: Path-loss versus the Tx-Rx distance in the measured mechanical room at the frequency $f = 2.45\,\mathrm{GHz}$.
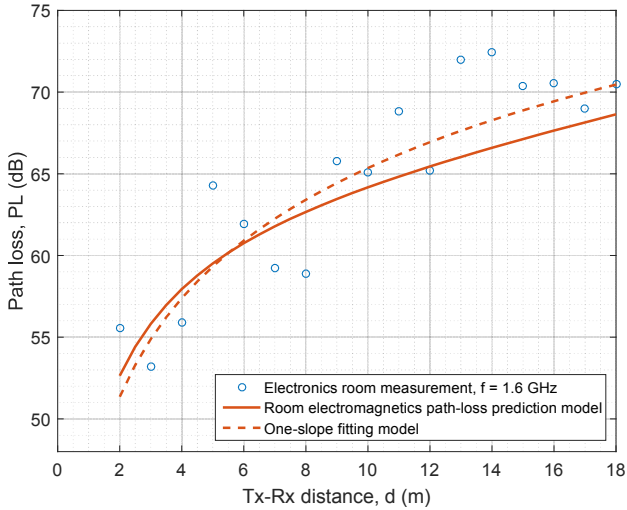

Fig. 11: Path-loss versus the Tx-Rx distance in the measured electronics room at the frequency $f = 1.60\,\mathrm{GHz}$.
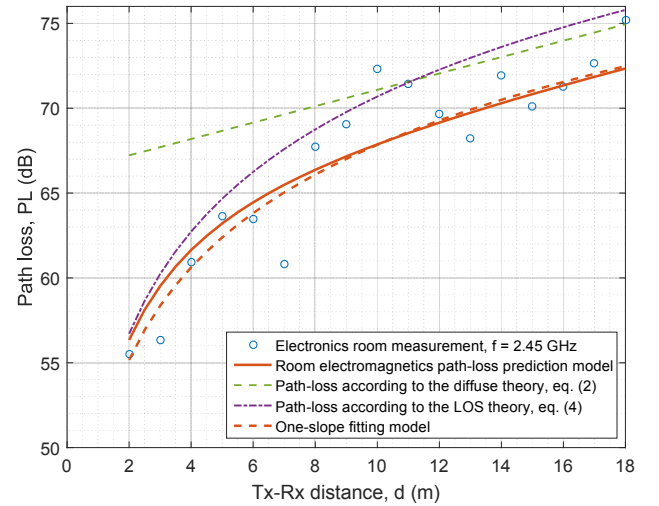

Fig. 12: Path-loss versus the Tx-Rx distance in the measured electronics room at the frequency $f = 2.45\,\mathrm{GHz}$.

B. Model Validation: Path-Loss

Figures 9 and 10 show the comparison of the measured path-loss along different Tx-Rx distances and the predicted path-loss based on the room electromagnetics theory for the mechanical room. The two figures correspond to the path-loss at 1.6 and 2.45 GHz in the investigated industrial room, respectively. It can be seen that the room electromagnetics theory based model gives very good prediction on path-loss along distances. It should be noted that the empirical path-loss model are often simply least square fit models which utilize the information from all data of a path-loss measurement [5]–[7]. Then, deriving those models are more about mathematical fitting to available data. However, the path-loss model presented in this paper is a truly predictive model derived based on the room electromagnetics and diffuse theory. Among the advantages of this approach is the simplicity and speed of the algorithm. It requires only one measurement of the PDP at any Tx-Rx distance regardless of the propagation scenarios (LOS

or NLOS), which is extremely time and cost efficient. It can also be seen from both the measurements and the prediction that the path-loss at 2.45 GHz is slightly higher than that at 1.6 GHz, which will be reconfirmed in the following path-loss versus frequency results. The same information are plotted for the electronics room measurement in Figs. 11 and 12. The results for the electronics room also show good agreement between the predicted path-loss and measurements. In Fig. 12, both the exponential law for the diffuse radiation according to (2) and the power law of LOS component in (4) are shown. It can be seen that the LOS component dominates before some threshold Tx-Rx distance, after which the diffuse part dominates.

To quantify the goodness-of-fit of the model, the deviation samples $\mathcal{D}_{i,j}$ in decibel unit between the predicted path-loss using the room electromagnetics based approach and the measured results at a given frequency f are calculated
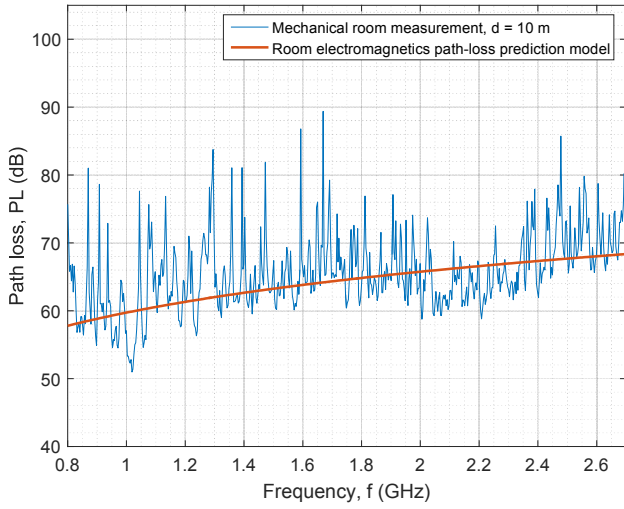
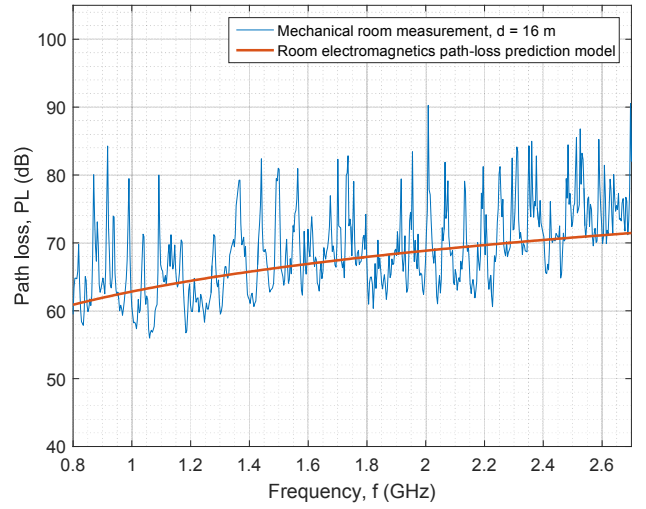Fig. 13: Path-loss versus the transmit frequency in the measured mechanical room at the Tx-Rx distance $d = 10\,\text{m}$.

Fig. 14: Path-loss versus the transmit frequency in the measured mechanical room at the Tx-Rx distance $d = 16\,\text{m}$.
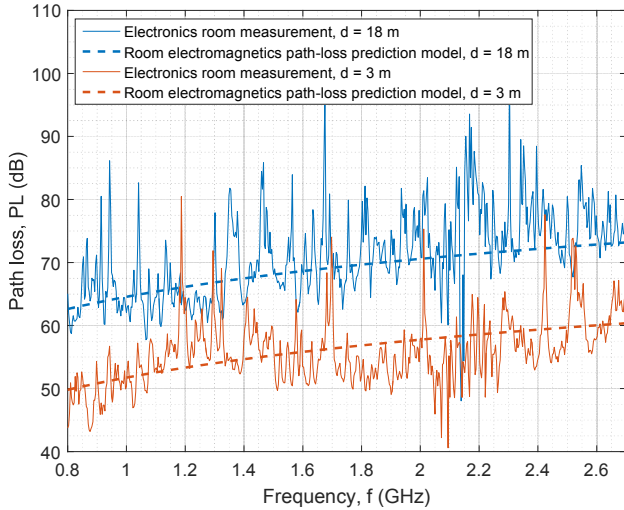

Fig. 15: Path-loss versus the transmit frequency in the measured electronics room at different Tx-Rx distances.
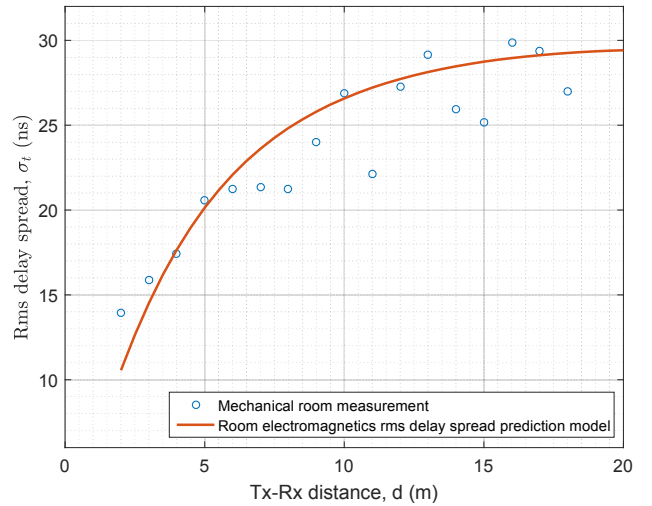

Fig. 16: Rms delay spread versus the Tx-Rx distance in the measured mechanical room.

TABLE I: Quantification Table of Goodness-of-Fit

Measurement scenario	One-slope model	Predicted model
M ($f = 1600$ MHz)	3.12 dB	3.25 dB
M ($f = 2450$ MHz)	3.15 dB	3.56 dB
E ($f = 1600$ MHz)	3.20 dB	3.45 dB
E ($f = 2450$ MHz)	2.85 dB	2.88 dB

according to the following expression:

$$\mathcal{D}_{i,j} = PL(d_i, f) - \mathcal{M}_j(d_i, f), \tag{13}$$

where $PL(d_i, f)$ is the path-loss at Tx-Rx distance d_i and frequency f predicted from the room electromagnetics approach or obtained from the one-slope model, $\mathcal{M}_j(d_i, f)$ represents the j-th path-loss measurement at the distance d_i and frequency f. After obtaining the deviation samples for

both methods, the root mean square error (RMSE) values are calculated and the results are shown in Table I, where **M** represents the mechanical room and **E** refers to the electronics room. It is observed that the RMSEs from the two approaches are quite close despite the fact that the one-slope model is fitted from a number of path-loss measurements while the room electromagnetics based approach only requires one measurement of the PDP.

Figures 13 and 14 illustrate the path-loss versus transmission frequency over the frequency range of 0.8 to 2.7 GHz in the mechanical room at the Tx-Rx distance of 10 m and 16 m, respectively. Despite the fluctuation due to small-scale fading, we can see that the room electromagnetics based model predict the path-loss versus transmission frequency quite well. From Figs. 13 and 14, the path-loss at the Tx-Rx distance $d = 16$ m is about 3 dB greater than that at $d = 10$ m. Additionally, a clear trend can be observed from both the measurements and prediction that the path-loss increases gradually along the transmission frequency at a fixed Tx-Rx distance. Figure

15 shows the predicted and measured path-loss at different frequencies at the Tx-Rx distance $d = 3$ m and the Tx-Rx distance $d = 18$ m. For the measurement at the former distance, the power from the LOS component is definitely dominant compared to the power resulting from the diffuse components; while the diffuse power is relatively larger for the Tx-Rx distance $d = 18$ m. For both cases, the room electromagnetic theory based prediction model gives a good estimate on the path-loss versus frequency.

C. Model Validation: Root Mean Square Delay Spread

Figure 16 shows the measured and predicted path-loss at different Tx-Rx distances in the mechanical room. It is observed that while the Tx-Rx distance is small, the rms delay spread increases quite quickly and it roughly has a linear relationship with the increasing Tx-Rx distance. When the Tx-Rx distance becomes larger, the increase rate of the rms delay spread along Tx-Rx distance decreases. This is explained by the expression of the K-factor in rms delay spread prediction function in (10), which is determined by power-law term of the Tx-Rx distance d in the denominator and the exponential term of the distance d in the nominator. The room electromagnetic based rms delay spread model provides a complete and accurate prediction function on the parameter, which complements the simple power-law relationship between the rms delay spread and Tx-Rx distance proposed in [29].

V. Conclusion

A path-loss and rms delay spread estimation algorithm based on the room electromagnetics theory is investigated. The room electromagnetics theory interprets the room as a cavity and considers the use of finite pulse width to excite the impulse response, which results in a spatial uniformly distributed diffuse power. The room electromagnetics theory is also a power based approach since all phase and polarization information is neglected. However, these characteristic parameters are supposed to be totally random in rooms with rough surfaces and dense scatters. This leads to the fact that the reverberation time can be considered as a constant over a certain frequency bands, which is verified with the measurements.

The prediction algorithm based on the room electromagnetics theory is extremely simple and effective. It requires only one measurement of the PDP with some easily accessible information on the investigated room. The path-loss characteristics of two large industrial halls have been analyzed experimentally and theoretically with the room electromagnetics based approach. The measured environments are big in size compared to office environments. Additionally, the measured industrial scenarios also present as highly scattered and occupied environments. The measurement results show that the tails of PDPs in one room have the same slope regardless of the Tx-Rx distance as well as propagation condition (LOS or NLOS). The predicted path-loss results are found to match the measurements very well within a few dB.

Future research includes verification and extension of the proposed approach in higher frequency range.

Appendix A
Path-Loss Prediction

Resulting from the complete randomness of the incoherent scatter, it is reasonable to assume uniform distribution for the energy radiance $I\,(\mathrm{W/(m^2 \cdot s)})$ at any time instant. Based on the definition of the energy density and the fact that the mean values of electric and magnetic energies are equal in the far field, the density W for one incident path in the direction (θ, φ) is related to the radiance $I(\theta, \varphi)$ along the same direction as follows [30]:

$$W(\theta, \varphi) = \frac{\varepsilon}{2}|E|^2 + \frac{1}{2\mu}|B|^2 = \frac{I(\theta, \varphi)}{c}, \qquad (\text{A-1})$$

where E and B represent the electric and magnetic field vectors, respectively, ε is the permittivity of the medium in which the field exists, μ is the magnetic permeability, and c denotes the velocity of the electromagnetic wave.

Since the radiance $I(\theta, \varphi)$ is uniformly distributed over space in the totally diffuse field we investigate, namely, $I(\theta, \varphi) = I_0$, we can obtain the total energy density by integrating $W(\theta, \varphi)$ over all directions, i.e.,

$$\begin{aligned} W &= \int_0^{2\pi}\int_0^{\pi} W(\theta, \varphi) \cdot \sin(\theta)\, d\theta d\varphi \\ &= \int_0^{2\pi}\int_0^{\pi} \frac{I_0 \cdot \sin(\theta)}{c}\, d\theta d\varphi = \frac{4\pi \cdot I_0}{c}. \end{aligned} \qquad (\text{A-2})$$

The increased power P_{ins} per second in the room is simply the product of the volume and the gradient of the total energy along the time, i.e.,

$$P_{ins} = \frac{dW}{dt} \cdot V. \qquad (\text{A-3})$$

Then, the total energy of the diffuse radiation in the room equals the product of the total energy density W in (A-2) and the space volume of the room V[1]. Assuming that the energy is incident on the surrounding wall and objects with area A, which absorbs η of the total energy. The absorbed energy is obtained by integrating the energy density over a half space as following:

$$P_{abs} = \int_0^{2\pi}\int_0^{\frac{\pi}{2}} \eta A \cdot I(\theta, \varphi) \cdot \cos(\theta) \cdot \sin(\theta)\, d\theta d\varphi = \eta A I_0 \pi. \qquad (\text{A-4})$$

In (A-4), the sine term results from the integration over the space while the cosine term stems from the definition of the apparent aperture in the direction θ [19]. Introducing the concept of effective absorption area analogous to the radar cross section in radar applications [31], i.e., $A' = \eta A$, with η being the absorption ratio and utilizing the relationship in (A-2), the absorbed energy in (A-4) can be rewritten as

$$P_{abs} = \pi A' \cdot I_0 = \frac{cA'W}{4}. \qquad (\text{A-5})$$

Let the input power be $P_{in}(t)$, it is balanced by the increased power P_{ins} given in (A-3) and the decreased power due to the

---

[1]For some indoor environments (e.g., the industrial facility), a considerable portion of the space in the room is occupied by other objects (e.g., the machineries), which should be excluded from the volume V when doing the calculations.

absorption of the wall in (A-5). This balance is mathematically expressed as:

$$P_{in}(t) = P_{ins} + P_{abs} = \frac{dW}{dt} \cdot V + \frac{cA'W}{4}. \quad \text{(A-6)}$$

The above formula is in good accordance with the acoustical equation for room acoustic [32], except for the acoustic case, the velocity is for sound while the velocity of electromagnetic wave is used in our scenario.

Setting $P_{in}(t) = 0$, the equation in (A-6) degrades to a homogeneous equation, and the solution is given as

$$W(t) = \frac{4P_{in}}{cA'} \cdot e^{-\frac{t}{\tau}}. \quad \text{(A-7)}$$

where τ is expressed as

$$\tau = \frac{4V}{cA'} = \frac{4V}{cA\eta}, \quad \text{(A-8)}$$

which is called the electromagnetic 'reverberation time' analogous to the time constant in the acoustic case derived by the Sabine's law [32]. It can be seen that the reverberation time is dependent only on the ratio of the volume of the room to the effective area. The reverberation time for the room electromagnetic analysis is further discussed in [28]. The reverberation time is also linked to the slope of the power-delay-profile (PDP) in dB as follows [28]:

$$\tau = -\frac{10 \cdot \log_{10} e}{s}, \quad \text{(A-9)}$$

where s denotes the slope of the PDP in dB (see Fig. 1.(b)).

For general values of P_{in}, there exists no closed-form solution to the differential function in (A-6) and a general solution is available as a convolution integral as follows:

$$W(t) = \frac{1}{V} \cdot \int_0^\infty P_{in}(t - t') \cdot e^{-\frac{t}{\tau}} dt'. \quad \text{(A-10)}$$

For the special case of input signal being a rectangular pulse of unit amplitude and width w, the solution in (A-10) can be expressed as

$$W(t) = \frac{4(e^{\frac{w}{\tau}} - 1)e^{-\frac{t}{\tau}}}{cA'}. \quad \text{(A-11)}$$

In practical wideband measurement, the pulse width w is typically much smaller than the reverberation time τ, then we have

$$W(t) = \begin{cases} \frac{4w}{c\tau A'} \cdot e^{-\frac{t}{\tau}} & \text{if } t \geq \frac{d}{c} \\ 0 & \text{if } t < \frac{d}{c}, \end{cases} \quad \text{(A-12)}$$

where d is the distance between the transmitter (Tx) antenna and the receiver (Rx) antenna, and the second subequation is because of the causality since no electromagnetic wave arrives at the Rx before the time instance $\frac{d}{c}$.

Utilizing the relationship in (A-2), the irradiance $\mathcal{I}(t)$ arriving at the Rx antenna at time instant t is given as

$$\mathcal{I}(t) = \begin{cases} \frac{w}{\pi \tau A'} \cdot e^{-\frac{t}{\tau}} & \text{if } t \geq \frac{d}{c} \\ 0 & \text{if } t < \frac{d}{c}. \end{cases} \quad \text{(A-13)}$$

Then, the total power received at the antenna is obtained by integrating the product of the irradiance and the absorption cross section area A'_1 and a polarization factor η_{pol} of the receiving antenna over the receiving time. It is straightforward to show that $A'_1 = \frac{\lambda^2}{4\pi}$ due to the fact that the distributed directional gain of any lossless antenna is 1 in a uniform, random environment [25]; and η_{pol} equals $\frac{1}{2}$ because the power is equally divided between two orthogonal polarizations and the antenna only receives half of the incident energy. Finally, the received diffuse power, P_{dif}, at the antenna can be expressed as

$$P_{dif} = \int_{\frac{d}{c}}^\infty A'_1 \eta_{pol} \cdot \mathcal{I}(t) \, dt = \frac{\lambda^2}{8\pi} \cdot \int_{\frac{d}{c}}^\infty \mathcal{I}(t) \, dt$$
$$= \frac{\lambda^2 w}{8\pi^2 \tau A'} \cdot \int_{\frac{d}{c}}^\infty e^{-\frac{t}{\tau}} \, dt = \frac{\lambda^2 w}{8\pi^2 A\eta} \cdot e^{-\frac{d}{c\tau}}. \quad \text{(A-14)}$$

APPENDIX B
ROOT MEAN SQUARE DELAY SPREAD PREDICTION

We fist derive the mean delay from the PDP. According to the definition, the mean delay $u_t(d)$ at the Tx-Rx distance d can be expressed as follows:

$$u_t(d) = \frac{\int_0^\infty t \cdot A_c(t) \, dt}{\int_0^\infty A_c(t) \, dt} = \frac{I_2}{I_1}. \quad \text{(A-15)}$$

It is straightforward to show that the integral I_1 is simply the sum of the diffuse power P_{dif} in (2) and the LOS power P_{dir} in (4) and can be expressed as

$$I_1 = P_{dir} + P_{dif} = \frac{P_{in} D_t D_r \lambda^2}{(4\pi d)^2} + \frac{P_{in} \lambda^2}{8\pi^2 A\eta} \cdot \exp\left(-\frac{d}{c\tau}\right). \quad \text{(A-16)}$$

The integral I_2 is solved as

$$I_2 = \frac{P_{in} D_t D_r \lambda^2}{(4\pi d)^2} \cdot \frac{d}{c} + \frac{P_{in} \lambda^2}{8\pi^2 A\eta\tau} \cdot \int_{\frac{d}{c}}^\infty t \cdot \exp\left(-\frac{d}{c\tau}\right) dt$$
$$= \frac{P_{in} D_t D_r \lambda^2}{(4\pi d)^2} \cdot \frac{d}{c} + \frac{P_{in} \lambda^2}{8\pi^2 A\eta} \cdot \left(\frac{d}{c} + \tau\right) \cdot \exp\left(-\frac{d}{c\tau}\right). \quad \text{(A-17)}$$

Substituting (A-16) and (A-17) into (A-15), the mean delay can be expressed as

$$u_t(d) = \frac{P_{dir} \cdot \frac{d}{c} + P_{dif} \cdot (\frac{d}{c} + \tau)}{P_{dir} + P_{dif}} = \frac{d}{c} + \frac{P_{dif}}{P_{dir} + P_{dif}} \cdot \tau. \quad \text{(A-18)}$$

Noticing that the ratio between the LOS power P_{dir} and the diffuse power P_{dif} is the well-known Ricean K-factor, i.e.,

$$K = \frac{P_{dir}}{P_{dif}} = \frac{D_t D_r A \cdot \eta}{2d^2 \cdot \exp(-\frac{d}{c\tau})}. \quad \text{(A-19)}$$

From (A-19), it can be seen that the value of K approaches infinity while the Tx-Rx distance d decreases to 0, and the K-factor becomes 0 when the distance goes to infinity.

Then, the mean delay can be further expressed as

$$u_t(d) = \frac{d}{c} + \frac{\tau}{K+1}. \quad \text{(A-20)}$$

The rms delay spread $\sigma_t(d)$ at the Tx-Rx distance d is computed, by definition, as

$$\sigma_t(d) = \sqrt{\frac{\int_0^\infty (t - u_t(d))^2 \cdot A_c(t) \, dt}{\int_0^\infty A_c(t) \, dt}} = \sqrt{\frac{I_3}{I_1}}. \quad \text{(A-21)}$$

Utilizing the same rationale and after some straightforward mathematical induplications, the rms delay spread can be expressed in terms of the K-factor as

$$\sigma_t(d) = \frac{\tau}{\sqrt{K+1}}. \qquad \text{(A-22)}$$

ACKNOWLEDGMENT

REFERENCES

[1] J. B. Andersen, T. S. Rappaport, and S. Yoshida, "Propagation measurements and models for wireless communications channels," *IEEE Communications Magazine*, vol. 33, no. 1, pp. 42–49, 1995.

[2] J. B. Andersen, K. L. Chee, M. Jacob, G. F. Pedersen, and T. Kürner, "Reverberation and absorption in an aircraft cabin with the impact of passengers," *IEEE Transactions on Antennas and Propagation*, vol. 60, no. 5, pp. 2472–2480, 2012.

[3] Y. Ai, M. Cheffena, and Q. Li, "Power delay profile analysis and modeling of industrial indoor channels," in *Proc. of European Conference on Antennas and Propagation (EuCAP)*. IEEE, 2015, pp. 1–5.

[4] E. Tanghe, D. Gaillot, M. Liénard, L. Martens, and W. Joseph, "Experimental analysis of dense multipath components in an industrial environment," *IEEE Transactions on Antennas and Propagation*, vol. 62, no. 7, pp. 3797–3805, 2014.

[5] R. Janaswamy and J. B. Andersen, "Path loss predictions in urban areas with irregular terrain topography," *Wireless Personal Communications*, vol. 12, no. 3, pp. 255–268, 2000.

[6] E. Tanghe, W. Joseph, L. Verloock, L. Martens, H. Capoen, K. V. Herwegen, and W. Vantomme, "The industrial indoor channel: large-scale and temporal fading at 900, 2400, and 5200 MHz," *IEEE Transactions on Wireless Communications*, vol. 7, no. 7, pp. 2740–2751, 2008.

[7] C. Oestges, D. Vanhoenacker-Janvier, and B. Clerckx, "Channel characterization of indoor wireless personal area networks," *IEEE Transactions on Antennas and Propagation*, vol. 54, no. 11, pp. 3143–3150, 2006.

[8] T. Olasupo, C. E. Otero, K. O. Olasupo, and I. Kostanic, "Empirical path loss models for wireless sensor network deployments in short and tall natural grass environments," vol. 64, no. 9, pp. 4012 – 4021, 2016.

[9] M. R. Akdeniz, Y. Liu, M. K. Samimi, S. Sun, S. Rangan, T. S. Rappaport, and E. Erkip, "Millimeter wave channel modeling and cellular capacity evaluation," *IEEE Journal on Selected Areas in Communications*, vol. 32, no. 6, pp. 1164–1179, 2014.

[10] H. Masui, T. Kobayashi, and M. Akaike, "Microwave path-loss modeling in urban line-of-sight environments," *IEEE Journal on Selected Areas in Communications*, vol. 20, no. 6, pp. 1151–1155, 2002.

[11] R. He, Z. Zhong, B. Ai, and J. Ding, "An empirical path loss model and fading analysis for high-speed railway viaduct scenarios," *IEEE Antennas and Wireless Propagation Letters*, vol. 10, pp. 808–812, 2011.

[12] O. Franek, J. B. Andersen, and G. F. Pedersen, "Diffuse scattering model of indoor wideband propagation," *IEEE Transactions on Antennas and Propagation*, vol. 59, no. 8, pp. 3006–3012, 2011.

[13] G. Steinböck, T. Pedersen, B. H. Fleury, W. Wang, and R. Raulefs, "Distance dependent model for the delay power spectrum of in-room radio channels," *IEEE Transactions on Antennas and Propagation*, vol. 61, no. 8, pp. 4327–4340, 2013.

[14] S. Cheng, D. P. Gaillot, E. Tanghe, P. Laly, T. Demol, W. Joseph, L. Martens, and M. Liénard, "Polarimetric distance-dependent models for large hall scenarios," *IEEE Transactions on Antennas and Propagation*, vol. 64, no. 5, pp. 1907–1917, 2016.

[15] P. Paschalidis, J. Nuckelt, K. Mahler, M. Peter, A. Kortke, M. Wisotzki, W. Keusgen, and T. Kuerner, "Investigation of mpc correlation and angular characteristics in the vehicular urban intersection channel using channel sounding and ray-tracing," *IEEE Transactions on Vehicular Technology*, vol. 65, no. 8, pp. 5874 – 5886, 2016.

[16] G. Steinböck, M. Gan, P. Meissner, E. Leitinger, K. Witrisal, T. Zemen, and T. Pedersen, "Hybrid model for reverberant indoor radio channels using rays and graphs," *IEEE Transactions on Antennas and Propagation*, vol. 64, no. 9, pp. 4036 – 4048, 2016.

[17] E. M. Vitucci, F. Mani, V. Degli-Esposti, and C. Oestges, "Polarimetric properties of diffuse scattering from building walls: experimental parameterization of a ray-tracing model," *IEEE Transactions on Antennas and Propagation*, vol. 60, no. 6, pp. 2961–2969, 2012.

[18] T. Abbas, J. Nuckelt, T. Kürner, T. Zemen, C. F. Mecklenbräuker, and F. Tufvesson, "Simulation and measurement-based vehicle-to-vehicle channel characterization: Accuracy and constraint analysis," *IEEE Transactions on Antennas and Propagation*, vol. 63, no. 7, pp. 3208–3218, 2015.

[19] J. B. Andersen, J. Ø. Nielsen, G. Pedersen, G. Bauch, and M. Herdin, "Room electromagnetics," *IEEE Antennas and Propagation Magazine*, vol. 49, no. 2, pp. 27–33, 2007.

[20] J. B. Andersen, J. Ø. Nielsen, G. Bauch, and M. Herdin, "The large office environment-measurement and modeling of the wideband radio channel," in *Proc. of IEEE International Symposium on Personal, Indoor and Mobile Radio Communications (PIMRC)*, 2006, pp. 1–5.

[21] G. Steinböck, T. Pedersen, B. H. Fleury, W. Wang, and R. Raulefs, "Experimental validation of the reverberation effect in room electromagnetics," *IEEE Transactions on Antennas and Propagation*, vol. 63, no. 5, pp. 2041–2053, 2015.

[22] J. Ø. Nielsen, J. B. Andersen, G. F. Pedersen, and M. Pelosi, "On polarization and frequency dependence of diffuse indoor propagation," in *IEEE Vehicular Technology Conference (VTC-Fall)*, 2011, pp. 1–5.

[23] A. Bamba, M.-T. Martinez-Ingles, D. P. Gaillot, E. Tanghe, B. Hanssens, J.-M. Molina-Garcia-Pardo, M. Lienard, L. Martens, and W. Joseph, "Experimental investigation of electromagnetic reverberation characteristics as a function of UWB frequencies," *IEEE Antennas and Wireless Propagation Letters*, vol. 14, pp. 859–862, 2015.

[24] S. Stavrou and S. Saunders, "Review of constitutive parameters of building materials," in *Proc. of International Conference on Antennas and Propagation (ICAP)*. IET, 2003, pp. 211–215.

[25] R. Vaughan and J. B. Andersen, *Channels, Propagation and Antennas for Mobile Communications*. The Institution of Engineering and Technology, 2003, vol. 50.

[26] D. J. Panagopoulos, O. Johansson, and G. L. Carlo, "Evaluation of specific absorption rate as a dosimetric quantity for electromagnetic fields bioeffects," *PLoS ONE*, vol. 8, no. 6, p. e62663, 2013.

[27] A. Meijerink and A. F. Molisch, "On the physical interpretation of the Saleh-Valenzuela model and the definition of its power delay profiles," *IEEE Transactions on Antennas and Propagation*, vol. 62, no. 9, pp. 4780–4793, 2014.

[28] A. Bamba, W. Joseph, D. Plets, E. Tanghe, G. Vermeeren, L. Martens, J. B. Andersen, and J. Ø. Nielsen, "Assessment of reverberation time by two measurement systems for room electromagnetics analysis," in *Proc. of IEEE International Symposium on Antennas and Propagation (APSURSI)*, 2011, pp. 3113–3116.

[29] J. Karedal, S. Wyne, P. Almers, F. Tufvesson, and A. F. Molisch, "A measurement-based statistical model for industrial ultra-wideband channels," *IEEE Transactions on Wireless Communications*, vol. 6, no. 8, pp. 3028–3037, 2007.

[30] A. Ishimaru, *Electromagnetic Wave Propagation, Radiation, and Scattering*. Prentice Hall, 1991.

[31] R. Sullivan, *Radar Foundations for Imaging and Advanced Concepts*. The Institution of Engineering and Technology, 2004.

[32] H. Kuttruff, *Room Acoustics*. CRC Press, 2009.